A heteroleptic fused bi-cuboctahedral cluster

Rhone P. Brocha Silalahi, Tzu-Hao Chiu, Hao Liang, Samia Kahlal, Jean-Yves Saillard, C.W. Liu

A Heteroleptic Fused Bi-cuboctahedral $Cu_{21}S_2$ Cluster

Rhone P. Brocha Silalahi,[§] Tzu-Hao Chiu,[§] Hao Liang,[¥] Samia Kahlal,[¥] Jean-Yves Saillard,[¥]* and C. W. Liu [§]*

[§]Department of Chemistry, National Dong Hwa University No. 1, Sec. 2, Da Hsueh Rd. Shoufeng, Hualien 97401 (Taiwan R.O.C.) E-mail:chenwei@gms.ndhu.edu.tw

[¥]Univ Rennes, CNRS, ISCR-UMR 6226, F-35000 Rennes (France)

Abstract. A new dicationic cluster, $[Cu_{21}S_2\{S_2CN^nBu_2\}_9(C_2Ph)_6]^{2+}$, which $Cu_{21}S_2$ kernel consists of two S@Cu_{12} cuboctahedra sharing a triangular Cu_3 face is reported. Its waist part is bridged by three dithiocarbamate ligands, each in a hexaconnective, hexametallic (μ_3, μ_3) coordination pattern, an unprecedented feature in Cu nanocluster chemistry.

Keywords: copper cluster, fused bi-cuboctahedra, hyper coordination, dithiocarbamate

The coordination chemistry of ligands utilized in metal nanocluster (NC) production is critical in defining their metal arrangement and NC overall shape.[1] The peripheral ligands allow the metal kernel to serve as nano-building blocks for their self-assembly into a larger kernel structure.[2] Peripheral ligand versatility assists core arrangement through kernel aggregation or fusion processes.[3] In the case of Ag and Au NCs, larger kernel structures originate from the aggregation or fusion of smaller units, such as M_4, M_{13}, and M_{14} (M = metal atom).[3-8] Among them, the fusion of M_{13} centered icosahedra stabilized by thiolate, phosphine, and/or co-ligands, has been thoroughly studied.[9-12] Conversely, only a few examples of fused M_{13} centered cuboctahedra have been reported, such as $Au_{28}(TBBT)_{20}$,[13] $Au_{30}S(S\text{-}t\text{-}Bu)_{18}$,[14,15] $[Au_{24}(C{\equiv}CPh)_{14}(PPh_3)_4](SBF_6)_2$,[16] $Au_{30}(S\text{-}t\text{Bu})$[17] and $Au_{30-x}Ag_x(S\text{-}t\text{Bu})_{18}$.[18] On the other hand, although dithiocarbamate (dtc) metal complexes are known since 1907, [19] no fused or aggregated metal kernel has been reported with such ligands so far.[20-23]

We recently isolated the new NC $[Cu_{15}H_2(S_2CN^nBu_2)_6(C_2Ph)_6](PF_6)$ (abbreviated as **$Cu_{15}H_2$**) in high yields by reacting $[K\{S_2CN^nBu_2\}]$, $[Cu(CH_3CN)_4](PF_6)$, phenylacetylene, and $NaBH_4$.[24] **$Cu_{15}H_2$** is formed as an intermediate in the earlier reported two-electron copper superatom $[Cu_{13}(S_2CN^nBu_2)_6(C_2Ph)_4]^+$, whose metal kernel features a centered cuboctahedron.[25-27] Moreover, the inverse coordination clusters $[Cu_{12}(S)\{S_2CN^nBu_2\}_6(C{\equiv}CR)_4]$ (R= CO_2Me and CO_2Et) have been reported,[25] which were

obtained from the reaction of $[Cu_{13}(S_2CN^nBu_2)_6(C{\equiv}CR)_4]^+$ with a two-fold excess of dtc ligands at low temperature. $[Cu_{12}(S)\{S_2CN^nBu_2\}_6(C{\equiv}CR)_4]$ was structurally characterized as a sulfide-centered Cu_{12} cuboctahedron.[25] Herein, we show that the acid addition to **$Cu_{15}H_2$** or $[Cu_{12}(S)\{S_2CN^nBu_2\}_6(C{\equiv}CPh)_4]$ leads to NC decomposition, followed by fusion to form $[Cu_{21}S_2\{S_2CN^nBu_2\}_9(C_2Ph)_6](PF_6)_2$ (abbreviated **$Cu_{21}S_2$**), whose kernel contains two S-centered Cu_{12} cuboctahedra sharing a Cu_3 triangle. *To the best of our knowledge, the fused bi-cuboctahedral $Cu_{21}S_2$ kernel is unprecedented in copper NCs*.

$Cu_{21}S_2$ was first generated as an orange-red precipitate with a 15 % yield from the reaction of **$Cu_{15}H_2$** with two equiv. of CF_3COOH (TFA) in acetone (Scheme S1a) at room temperature. **$Cu_{21}S_2$** can also be synthesized in 20 % yield from reacting $[Cu_{12}S(S_2CN^nBu_2)_6(C_2Ph)_4]$ (abbreviated **$Cu_{12}S$**) with two equiv. of TFA and NBu_4PF_6 in chloroform at ambient temperature (Scheme S1b). The **$Cu_{12}S$** reactant was prepared in the same way as its $[Cu_{12}(S)\{S_2CN^nBu_2\}_6(C{\equiv}CR)_4]$ (R= CO_2Me and CO_2Et) relatives.[25] A third synthetic pathway is to directly synthesize **$Cu_{21}S_2$** by reacting $[Cu(CH_3CN)_4](PF_6)$, dtc ligands, phenylacetylene, a sulfur salt, and Et_3N in THF/CH_3CN at 50°C (Scheme S1c), with a 23 % yield.

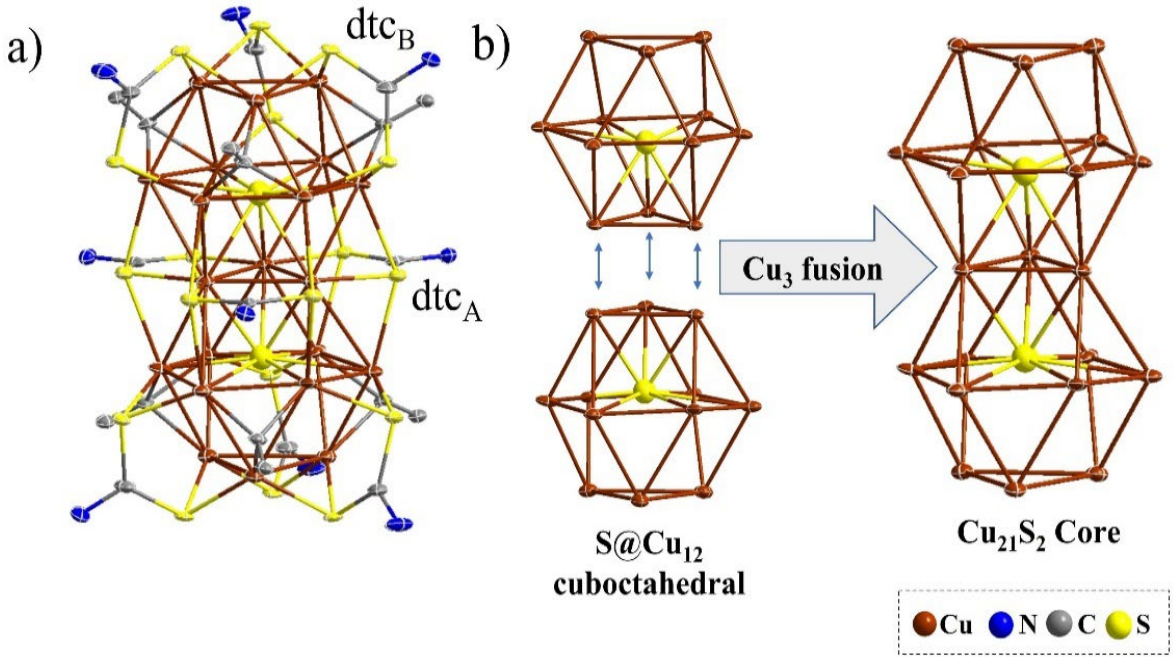

Figure 1. a) The crystal structure of **$Cu_{21}S_2$** with the n-butyl groups and phenyl rings omitted for clarity. b) Face-fused bi-cuboctahedral $S_2@Cu_{21}$ core.

$Cu_{21}S_2$ crystallizes in the trigonal space group P(-)31*c*. Its di-cation X-ray structure is shown in Figure 1, and metric data are provided in Tables 1 and S1. The whole cluster core, $S_2@Cu_{21}$, can be viewed as resulting from the fusion of two S-centered Cu_{12} cuboctahedra by sharing a Cu_3 triangle. In each $S@Cu_{12}$ cuboctahedron, three among the eight triangular faces are capped by alkynyl groups, each in a μ_3-η^1 fashion. The Cu-C distances (avg. 2.047(7) Å) are comparable to that in X-centered Cu_{12} (X= S, Cl, Br) cuboctahedral cores.[25] The nine dtc ligands exhibit two coordination patterns: types dtc_A and dtc_B. In type dtc_A, three dtc ligands act as a bridge joining the waist part of the bi-cuboctahedral **$Cu_{21}S_2$** kernel, *forming an unprecedented hexaconnective hexametallic (μ_3, μ_3) coordination pattern.* Thus, **$Cu_{21}S_2$** is the first cluster with a dtc ligand adopting a (μ_3, μ_3) coordination mode among ~ 5000 structures deposited in the CSDB.[27] The averaged Cu-(μ_3-S) distance is 2.3627(18) Å. In type dtc_B, six dtc ligands are connected in a (μ_2, μ_2) binding mode to the six square faces, three on each of the $S@Cu_{12}$ cuboctahedra, with average Cu-(μ_2-S) distances of 2.279(5) Å. They are comparable to the Cu-(μ_2-S) distances in a $S@Cu_{12}$ cuboctahedral relative (avg. 2.295 Å).[25] Interestingly, the encapsulated sulfides cannot bind to the twelve copper atoms of their respective cuboctahedral cage. Rather, they only bind to the nine in the most inner positions. Consequently, they are slightly pushed towards each other (lying at 3.888(3) Å off the Cu_6 hexagonal plane) but remain far apart (S···S = 4.1699(2) Å). The Cu-(μ_9-S) bond lengths are in the range of 2.4688(19)-2.8016(10) Å (avg. 2.6010(13) Å), i.e., comparable to the Cu-(μ_9-S) distances (avg. 2.554(2) Å) in $[Cu_{11}(\mu_9\text{-}S)(\mu_3\text{-}Br)_3\{(S_2P(O^iPr)_2\}_6]$,[28] and shorter than the Cu-(μ_{12}-S) bond lengths in $[Cu_{12}S\{S_2CN^nBu_2\}_6(C{\equiv}CCO_2Me)_4]$[25] (avg. 2.706 Å). The Cu-Cu distances in **$Cu_{21}S_2$** (range of 2.5995(8)-2.9906(16) Å; avg. 2.7285(11) Å) are consistent with weak Cu(I)-Cu(I) cuprophilic interactions. Besides, the copper atoms located on the two outer triangular faces are in an approximate planar trigonal coordination mode (CuS_2C). Those belonging to the shared triangular face are bonded to the two sulfides and two dtc sulfur atoms in a tetrahedral coordination mode. Those belonging to the Cu_6 hexagonal planes are also coordinated in a distorted tetrahedral arrangement, bonded to one sulfide, alkynyl carbon, and dtc sulfur atoms. As a result, the ideal symmetry of the **$Cu_{21}S_2$** is D_{3h}.

Table1. Selected experimental (X-ray) and DFT-computed data for **$Cu_{21}S_2$**. Values in brackets are the averaged Wiberg bond indices (WBIs). NAO = natural atomic orbital.

Distances(Å)	**X-ray**	**DFT**
Cu-C	2.012(7)-2.074(7) avg. 2.047(7)	2.020-2.064 avg 2.036 [0.216]
Cu-(μ_3-S)	2.3143(2)-2.4213(2) avg. 2.3627(18)	2.408-2.483 avg. 2.485 [0.157]
Cu-(μ_2-S)	2.2512(19)-2.333(2) avg. 2.279(5)	2.251-2.333 avg. 2.358 [0.225]
Cu-(μ_9-S)	2.4688(19)-2.8016(10) avg. 2.6010(13)	2.457-2.762 avg. 2.581 [0.096]
Cu-Cu	2.5995(8)-2.9906(16) avg. 2.7285(11)	2.573-2.769 avg. 2.656 [0.073]
NAO charges		
Cu_{shared}[a] x 3	--------	0.63
$Cu_{unshared}$[a] x 18	--------	0.70
$S_{sulfide}$ x 2	--------	-1.26

[a] Shared/unshared by the two face-sharing cuboctahedra.

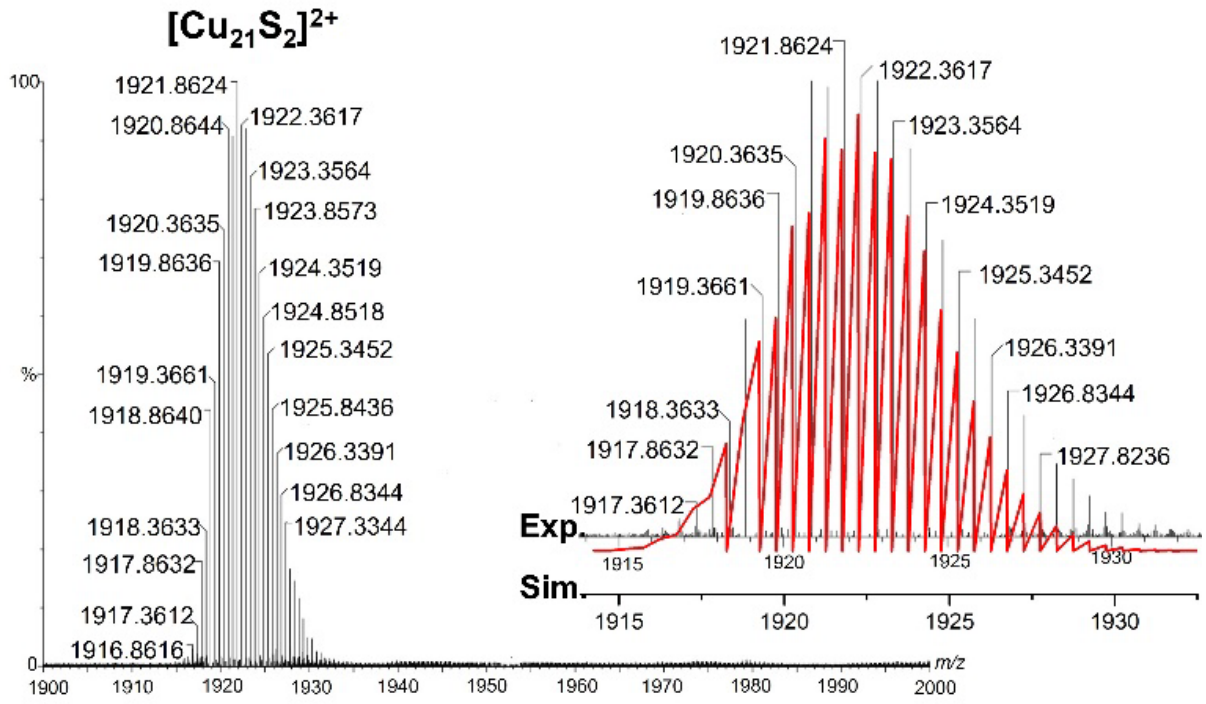

Figure 2. Mass spectrum of the **$Cu_{21}S_2$** cluster in positive mode. Inset: the comparison of measured (top) and simulated (bottom) isotopic pattern of the species $[Cu_{21}S_2\{S_2CN^nBu_2\}_9(C_2Ph)_6]^{2+}$.

The composition of **$Cu_{21}S_2$** was determined by electrospray ionization mass spectrometry (ESI-MS), which shows an intense peak with half-unit spacing at *m/z* 1921.86 Da, corresponding to the molecular ion $[Cu_{21}S_2\{S_2CN^nBu_2\}_9(C_2Ph)_6]^{2+}$ (calc. *m/z* at 1921.74 Da) (Figure 2). The experimental isotope pattern aligns with the simulated spectrum (Figure 2. Inset). Nuclear magnetic resonance (NMR) was carried out to identify the proton resonance corresponding to the alkyl group of dtc and alkynyl in **$Cu_{21}S_2$**. The ^{1}H NMR spectrum shows in well-defined splitting patterns the peak of *n*-butyl ligands with an integration ratio of 2:1 (Figure S1-S2). The ^{1}H NMR spectra exhibit peaks centered at 4.03 (-CH_2), 1.72 (-CH_2), 1.32 (-CH_2), and 0.86 (-CH_3) ppm correspond to the six dtc ligand along the C_3 axis, while the peaks centered at 4.22 (-CH_2), 1.89 (-CH_2), 1.42 (-CH_2), and 0.96 (-CH_3) ppm correspond to the three dtc ligand along the C_2 axis, and a set of chemical shifts assignable to the alkynyl ligands (7.43-7.61 ppm, C$_2$*Ph*), respectively. Each peak corresponds to the two types of coordination patterns of dtc ligands and is in line with the D_{3h} symmetry of **$Cu_{21}S_2$** structure. The ^{13}C NMR spectrum of **$Cu_{21}S_2$** clearly indicates a strong signal for each carbon atom in the alkynyl and dtc ligand,

as shown in Figure S3. The $^{31}P\{^{1}H\}$ NMR spectrum reveals a septet peak centered at -143.11 ppm, corresponding to the PF_6^- counter anion (Figure S4).

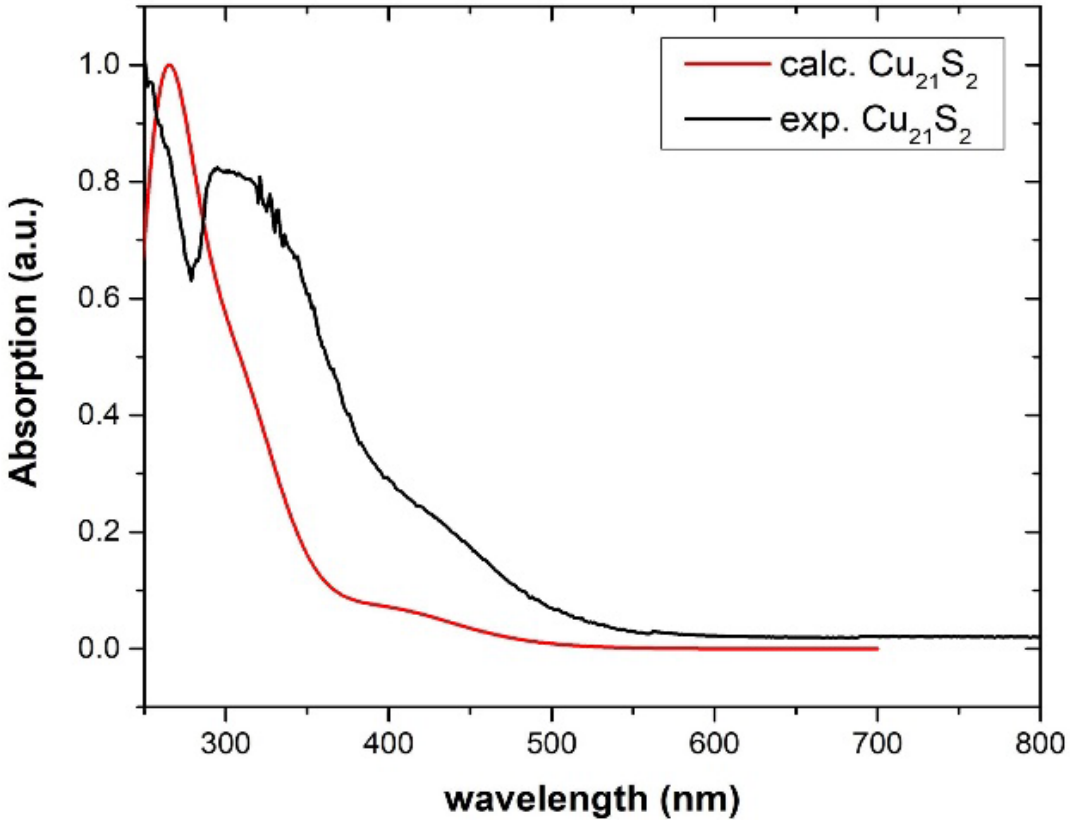

Figure 3. Experimental UV-vis absorption compared with the calculated spectrum of **$Cu_{21}S_2$**.

The UV-vis spectrum of the **$Cu_{21}S_2$** cluster (orange crystal dissolved in Me-THF) is shown in Figure 3. The absorption spectrum of the cluster exhibits two bands, a shoulder absorption at 430 nm and an intense band at 295 nm, which is quite similar to the calculated absorption spectrum at 392 and 300 nm (Figure 3). The UV-vis absorption spectrum of **$Cu_{21}S_2$** shows distinct bands to those observed in **$Cu_{15}H_2$** and **$Cu_{12}S$** (Figure S5). The absorption could be affected by transforming the core between the bi-capped icosahedron of **$Cu_{15}H_2$** into the fused bi-cuboctahedral **$Cu_{21}S_2$** core. Besides, the fusion assembly of two cuboctahedral **$Cu_{12}S$** into one bi-cuboctahedral **$Cu_{21}S_2$** core leads to a hypsochromic shift in the lowest energy absorption band upon going from **$Cu_{12}S$** (457 nm) to **$Cu_{21}S_2$** (430 nm).

As mentioned above, the reaction of two equiv. TFA with **$Cu_{15}H_2$** and **$Cu_{12}S$** led to the metal kernel transformation. In the case of **$Cu_{15}H_2$**, the added acid triggers the degradation of **$Cu_{15}H_2$** and provoke a C-S(dtc) bond cleavage. A probable degradation pathway from **$Cu_{15}H_2$** into **$Cu_{21}S_2$** can be categorized into a multiple-step degradation process, such as disconnecting the encapsulated linear $[CuH_2]^-$ unit followed by the C-S bond cleavage, removing two

[CuC_2Ph] units, and the fusion of two **$Cu_{12}S$** cuboctahedra to form **$Cu_{21}S_2$**. To summarize, the bi-capped icosahedral **$Cu_{15}H_2$** core progressively decomposes into a **$Cu_{12}S$** cuboctahedron core, followed by the assembly of two **$Cu_{12}S$** cuboctahedra to generate a fused bi-cuboctahedral **$Cu_{21}S_2$** core (Scheme S2). Of note, the **$Cu_{15}H_2$** degradation in acidic conditions occurs in a slightly different pathway than in chloro-solvents at elevated temperatures.[24]

Time-dependent ^{1}H NMR spectroscopy was carried out to assess the degradation of **$Cu_{15}H_2$** in acidic conditions. The two sets of the ^{1}H NMR chemical shifts of the dtc alkyl groups have shifted downfield (Figure S6). This result is accompanied by the liberation of H_2 ($\delta = 4.59$ ppm). This is corroborated by the ESI-MS spectra (Figure S7). We propose that **$Cu_{15}H_2$** (A = *m/z* at 2789.27 Da) disintegrates to $[Cu_{13}S\{S_2CN^nBu_2\}_6(C_2Ph)_5{+}H^+]^+$ (B = *m/z* at 2589.36 Da) by the cleavage of the linear $[CuH_2]^-$ unit encapsulated within its Cu_{14} host, eliminating [CuC_2Ph], and accompanied by a sulfide formation. The disintegration continues by cleaving out a [CuCPh] unit to form $[Cu_{12}S\{S_2CN^nBu_2\}_6(C_2Ph)_4{+}H^+]^+$ (C = *m/z* at 2426.39 Da). In the last stage, **$Cu_{12}S$** undergoes the fusion of two sulfide-centered cuboctahedra to generate the fused bi-cuboctahedral $[Cu_{21}S_2\{S_2CN^nBu_2\}_9(C_2Ph)_6]^{2+}$. All the observed isotopic patterns of the fragment peak, A, B, and C, align with the simulated ones (Figure S8-S10).

Scheme S3 depicts the **$Cu_{12}S$** degradation pathway under acidic conditions. The **$Cu_{12}S$** cuboctahedron undergoes the fusion of two **$Cu_{12}S$** cuboctahedra in the bi-cuboctahedral **$Cu_{21}S_2$**. Time-dependent ^{1}H NMR spectroscopy investigated the degradation of **$Cu_{12}S$** after TFA addition in *d_6*-acetone (Figure S11). Upon examining the ^{1}H NMR spectrum, the dtc *n*-butyl signals appear to be splitted into two sets, in accordance with what is observed in the ^{1}H NMR spectrum of **$Cu_{21}S_2$** (Figure S12). The results agree with our UV-vis experiments in $CHCl_3$, showing that **$Cu_{12}S$** is converted into **$Cu_{21}S_2$** by assembling two **$Cu_{12}S$** cuboctahedra in acidic conditions. The initial absorption spectrum of **$Cu_{12}S$** is gradually blue-shifted, (Figure S13). The low energy band at 457 nm is shifted to 435 nm, while the high energy band at 325 nm is shifted to 300 nm, corresponding to the absorption bands of **$Cu_{21}S_2$** at 295 and 430 nm (Figure 3). We investigated the luminescent properties of **$Cu_{21}S_2$** in both solution and solid states and found that only **$Cu_{12}S$** displays photoluminescence in both solids and solutions at 77 K.[25] On the other hand, **$Cu_{15}H_2$** and **$Cu_{21}S_2$** are non-emissive (Figure S14). Presumably the lower rigidity of **$Cu_{21}S_2$**, resulting from the fusion of two $S@Cu_{12}$ cuboctahedra, quenches the emission.[29-30]

Density functional theory (DFT) calculations were carried out at BP86/def2-SVP level (see Computational Details) to shed some light on the bonding in **$Cu_{21}S_2$**. In order to reduce the computational cost, the $S_2CN^nBu_2$ ligands were replaced by S_2CNH_2. Selected computed

data are given in Table 1. The optimized geometry of **$Cu_{21}S_2$** is in good agreement with its X-ray counterparts (Table 1). Its Kohn-Sham MO diagram (Figure S15) exhibits a large HOMO-LUMO gap consistent with its stability. The highest occupied orbitals have a major metal character, whereas the lowest unoccupied ones are ligand-centered. The computed natural atomic orbital (NAO) charges of the three Cu atoms, which are shared between the two cuboctahedra (+0.63), are lower than that of the other Cu atoms, which all equal +0.70. Nevertheless, all these charges are consistent with the +I oxidation state of Cu,[25] as well as the small Cu-Cu Wiberg bond indices (Table 1), which are indicative of weak cuprophilic (d^{10}-d^{10}) interactions.[24-27] The sulfide NAO charge (-1.26) is consistent with iono-covalent bonding.

Time-dependent DFT (TD-DFT) calculations performed at the CAM-B3LYP/def2-SVP level (see Computational details) allowed to simulate satisfyingly the UV-vis spectrum (Figure 3a), with a low energy shoulder centered around 392 nm and a high energy peak at 300 nm. The former corresponds to transitions from lower occupied MOs of significant metal character to the LUMO (MLCT), and the latter can be described as a combination of the HOMO-2 → LUMO+1 and HOMO-2 → LUMO+2 transitions, *i.e.* of MLCT character with some sulfide-to-dtc admixture).

In summary, we have successfully isolated and characterized **$Cu_{21}S_2$** from the reaction of cluster templates **$Cu_{15}H_2$** and **$Cu_{12}S$** with two equiv. of TFA, where the isolated yield can be improved by the one-pot reaction method. The addition of acid leads to the structural degradation of the template cluster, which disconnects the linear $[CuH_2]^-$ unit, cleaves out two $[CuC_2Ph]$ units and assembles two cuboctahedra to form a fused bi-cuboctahedral $Cu_{21}S_2$ kernel. We expect to produce more copper clusters of this kind via the fusion of two halide-centered Cu_{12} cuboctahedral structures, $[X@Cu_{12}(dtc/dtp)_6(C_2Ph)_4]^+$ (X = Cl, Br, I),[25,31] after working out appropriate synthetic conditions.

Conflicts of interest

"There are no conflicts to declare".

References

1 J. Yan, B. K. Teo, and N. Zheng. *Acc. Chem. Res*., 2018, **51**, 3084-3093.

2 X. Kang, and M. Zhu. *Coord. Chem. Rev.,* 2019, **394**, 1-38.

3 X. Du, J. Chai, S. Yang, Y. Li, T. Higaki, S. Li, and R. Jin. *Nanoscale,* 2019, **11**, 19158-19165.

4 X. Kang, and M. Zhu. *Coord. Chem. Rev*., 2019, **394**, 1-38.
5 S. Kenzler, and A. Schnepf. *Chem. Sci.,* 2021, **12**, 3116-3129.
6 X. Kang,and M. Zhu. *Chem Mater*., 2021, **33**, 39-62.
7 X. Kang, and M. Zhu. *Chem. Mater*., 2019, **31**, 9939−9969.
8 H. Hirai, S. Ito, S. Takano, K. Koyasu, and T. Tsukuda. *Chem. Sci.,* 2020, **11**, 12233-12248.
9 S. Jin, S. Wang, and M. Zhu. *Chem. Asian. J.,* 2019, **14**, 3222-3231.
10 T.-H. Chiu, J.-H. Liao, F. Gam, I. Chantrenne, S. Kahlal, J.-Y. Saillard, and C. W. Liu. *J. Am. Chem. Soc.,* 2019, **141**, 12957-12961.
11 D. Yang, and Y. Zhu. *Chin. J. Catal*., 2021, **42**, 245-250.
12 C. Xu, Y. Zhou, J. Yi, D. Li, L. Shi, and L. Cheng. *J. Phys. Chem. Lett.,* 2022, **13**, 1931-1939.
13 C. Zeng, T. Li, A. Das, N. L. Rosi, and R. Jin. *J. Am. Chem. Soc*., 2013, **135**, 10011−1001.
14 X.-K. Wan, W. W. Xu, S.-F. Yuan, Y. Gao, X.-C. Zeng, and Q.-M. Wang. *Angew. Chem. Int. Ed*., 2015, **54**, 9683 –9686.
15 H. Yang, Y. Wang, A. J. Edwards, J. Yan, and N. Zheng. *Chem. Commun*., 2014, **50**, 14325-14327.
16 D. Crasto, S. Malola, G. Brosofsky, A. Dass, and H. Hakkien. *J. Am. Chem. Soc.,* 2014, **136**, 5000−5005.
17 A. Dass, T. Jones, M. Rambukwella, D. Crasto, K. J. Gagnon, L. Sementa, M. D. Vetta, O. Baseggio, E. Apra, M. Stener, and A. Fortunelli. *J. Phys. Chem. C.,* 2016, **120**, 6256−6261.
18 K. H. Wijesinghe, N. A. Sakthivel, T. Jones, and A. Dass. *J. Phys. Chem. Lett*., 2020, **11**, 6312−6319.
19 G. Hogarth, Transition Metal Dithicarbamates: 1978-2003. In Progress in Inorganic Chemistry, K. D. Karlin. 2005, vol. 53, pp. 71-561. https://doi.org/10.1002/0471725587.ch2
20 A. J. Edwards, R. S. Dhayal, P.-K. Liao, J.-H. Liao, M.-H. Chiang, R. O. Piltz, S. Kahlal, J.-Y. Saillard, and C. W. Liu. *Angew. Chem. Int. Ed.*, 2014, **53**, 7214-7218.
21 P.-K. Liao, C.-S. Fang, A. J. Edwards, S. Kahlal, J.-Y. Saillard, and C. W. Liu. *Inorg. Chem.,* 2012, **51**, 12, 6577–6591.
22 R. P. B. Silalahi, J.-H. Liao, Y.-F. Tseng, T.-Z. Chiu, S. Kahlal, J.-Y. Saillard, and C.W. Liu. *Dalton Trans*., 2023, **52**, 2106-2114.

23 P. V. V. N. Kishore, J.-H. Liao, H.-N. Hou, Y.-R. Lin and C. W. Liu. *Inorg. Chem*. 2016, **55**, 7, 3663–3673.

24 K. K. Chakrahari, J. Liao, R. P. B. Silalahi, T.-H. Chiu, J.-H. Liao, X. Wang, S. Kahlal, J.-Y. Saillard, and C. W. Liu. *Small,* 2021, **17**, 2002544.

25 K. K. Chakrahari, R. P. B. Silalahi, J.-H. Liao, S. Kahlal, Y.-C. Liu, J.-F. Lee, M.-H. Chiang, J.-Y. Saillard, and C. W. Liu. *Chem. Sci*., 2018, **9**, 6785-6795.

26 R. P. B. Silalahi, K. K. Chakrahari, J._H. Liao, S. Kahlal, Y.-C. Liu, M.-H. Chiang, J.-Y. Saillard, and C. W. Liu. *Chem. Asian J*., 2018, **13**, 500 – 504.

27 K. K. Chakrahari, J.-H. Liao, S. Kahlal, Y.-C. Liu, M.-H. Chiang, J.-Y. Saillard, and C. W. Liu. *Angew. Chem. Int. Ed.,* 2016, **55**, 14704 –14708.

28 B. Li, J.-H. Liao, H.-T. Tang, Y.-J. Li, and C. W. Liu. *Dalton Trans*., 2013, **42**, 14384-14387.

29 Y. Zhong, J. Zhang, T. Li, W. Xu, Q. Yao, M. Li, X. Bai, Z. Wu, J. Xie, and Y. Zhang. *Nat Commun.*, 2023, **14**, 658. https://doi.org/10.1038/s41467-023-36387-2.

30 Z. Lei, P. Zhao, X.-L. Pei, H. Ube, M. Ehara, and M. Shionoya. *Chem. Sci.,* 2023, **14**, 6207-6215.

31 G.-R. Huang, R. P. B. Silalahi, J.-H. Liao, T.-H. Chiu, and C. W. Liu. *Dalton Trans*., 2022, **51**,15903-15911.

TOF

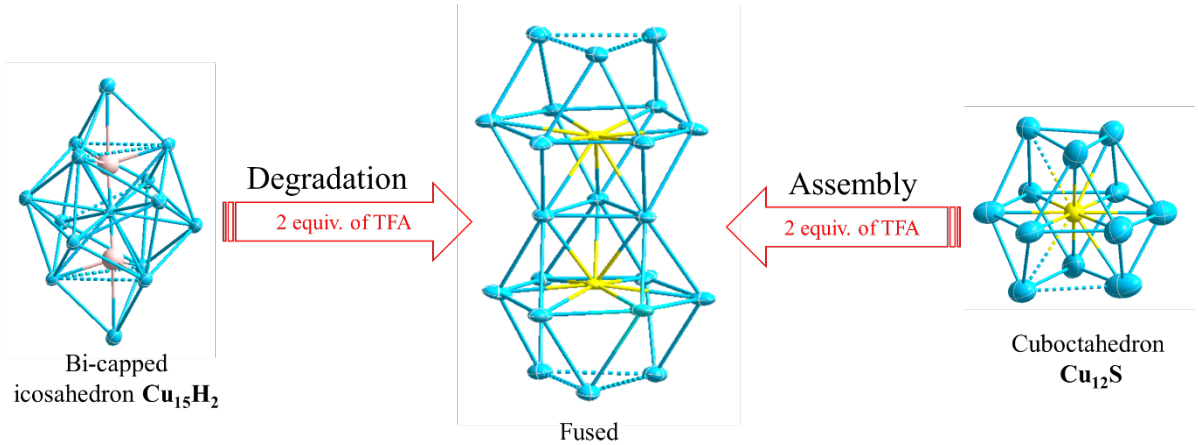

The addition of two equiv. of trifluoroacetic acid into the cluster templates **$Cu_{15}H_2$** or **$Cu_{12}S$** provokes the structural change of either the **$Cu_{15}H_2$** bicapped icosahedron or the **$Cu_{12}S$** cuboctahedron into the **$Cu_{21}S_2$** fused bi-cuboctahedron.